Engineering with Computers (2022) 38 (Suppl 2):S1243–S1254
https://doi.org/10.1007/s00366-020-01273-8

ORIGINAL ARTICLE

Multi-extremum-modified response basis model for nonlinear response prediction of dynamic turbine blisk

Behrooz Keshtegar[1,2,3] · Mansour Bagheri[4] · Cheng-Wei Fei[1] · Cheng Lu[1] · Osman Taylan[5] · Duc-Kien Thai[6]

Received: 2 July 2020 / Accepted: 28 December 2020 / Published online: 21 January 2021

Abstract

For the nonlinear dynamic analyses of complex mechanical components, it is necessary to apply efficient modeling framework to reduce computational burden. The accurate surrogate model for approximating the nonlinear responses of several failures is a vital issue to provide robust and safe design conditions in complex engineering applications. In this paper, two different Modified multi-extremum Response Surface basis Models (MRSM) are proposed for dynamic nonlinear responses of failure capacities for turbine blisk responses. The proposed MRSM is established using two regression processes including regressed the input variables by linear or exponential basis functions in first calibrating phase and regressed the second-order polynomial basis function using inputs data provided by first stage in second calibrating procedure. A sensitivity analysis using MRSM is proposed to consider the variation of input variables on the nonlinear responses. In the sensitivity analysis procedure, the effects of input variables are evaluated using the calibrating results given from the first regressed process. To evaluate the performance of the proposed MRSM, three multi-extremum failure modes including radial deformation of compressor blisk, maximum strain, and stress of compressor blade and disk are considered. the prediction of MRSM of nonlinear responses for Thermal-fluid–structure system with dynamical nonlinear finite-element analyses is compared with response surface method (RSM) and artificial neural network (ANN). The predicted results of modeling approaches showed that the sensitivity analysis based on MRSM accurately provided the effective degree for input variables. The gas temperature has the highest effects on nonlinear responses of turbine blisk which is followed by angular speed and material density. The MRSM combined with basic exponential function performs better than other models, while the MRSM coupled with linear function is more accurate than ANN and RSM. The proposed MRSM models have illustrated the accurate and efficient framework for approximating dynamic structural analysis of complex components.

Keywords Multi-extremum-modified response basis model · Turbine blisk · Multi-failure mode · Nonlinear dynamics · Sensitivity analysis

✉ Cheng-Wei Fei
cwfei@fudan.edu.cn

1 Department of Aeronautics and Astronautics, Fudan University, Shanghai 200433, People's Republic of China

2 Department of Civil Engineering, Faculty of Engineering, University of Zabol, P.B. 9861335856, Zabol, Iran

3 Institute of Research and Development, The Faculty of Civil Engineering, Duy Tan University, Da Nang 550000, Vietnam

4 Department of Civil Engineering, Birjand University of Technology, Birjand, Iran

5 Department of Industrial Engineering, Faculty of Engineering, King Abdulaziz University, P. O. Box 80204, Jeddah, Saudi Arabia

6 Department of Civil and Environmental Engineering, Sejong University, 98 Gunja-dong, Gwangjin-gu, Seoul 143-747, South Korea

1 Introduction

As a key part of an aeroengine, turbine blisk is applied to convert and transfer the energy, which significantly affects the efficiency and safety of aeroengine. As up to 25% of aeroengine failures are related to turbine blisk. Accurate design and estimation on the dynamic responses of turbine blisk are more critical for the growing demand for high-efficiency and safe aeroengines.

The mechanical evaluation of aeroengine components have emerged. Meguid et al. [1] studied bird strike resistance of an aeroengine applying explicit numerical approach and 3-D finite-element modeling. Results indicated that the significant effect on the impact force belongs to the first contact area between the bird and target of the first phase of the

impulse. Qi et al. presented a method to consider the boundary conditions and calculated the tip clearance of aeroengine considering the effects of rotation speed, pressure and temperature [2]. The main findings of this work include the main role of shaft speed on turbine disk displacement and temperature influence on turbine blade. Dong et al. investigated the effect of ice accretion and flowfield on the performance of an aeroengine structure. A comparison of the computational and experimental data showed acceptable agreement for strut temperature [3]. Szwaba et al. [4] examined the influence of aerodynamic characteristics and heat transfer of radial cooling passage walls of a turbine blade. Survey results indicated that transient method is easy to apply and its most important feature is that stable conditions in cooling walls are that stable conditions in wall temperature are not necessary to consider. Peschiulli et al. [5] proposed a methodology to investigate thermal characteristics and clearance control of complex mechanical system. Satish et al. [6] dynamically analyzed aeroengines blade-tip clearance (BTC) by an error identifying approaches to decrease system uncertainties.

For deterministic studies on the behavior and characteristics of aeroengine whole-body and components, various works on the probabilistic analysis of turbine blisk are conducted. Zhai et al. [7] developed a stochastic model updating (SMU) procedure using Monte Carlo (MC) method and an improved response surface method (RSM) for reliability analysis of aeroengines and complex structures, and showed that the SMU procedure could precisely simulate aeroengine system with desired efficiency. Lu et al. [8] developed Improved decomposed-coordinated Kriging modeling strategy for dynamic probabilistic analysis of multi-component structures with acceptable computational efficiency. Surrogate models are commonly used to optimization and RBDO of complex engineering problems [9, 10]. Machine-leaning basis nonlinear relations are successfully used to approximate the failure domains of probabilistic functions in structural reliability analyses. The call function as computational burden of the limit state function can be improved using hybrid reliability methods such as Kriging [11–18], response surface method [19], support vector machine [20–24], M5Tree [25, 26] and artificial neural network [27] in structural reliability design. Hu et al. [28] developed a low computational approach for the optimum design of turbine disk reliability using a single-loop-single-vector (SLSV) approach. Fei and Bai [29] proposed an efficient probabilistic numerical procedure based on support vector machine (SVM), and revealed the proposed approach with high efficiency and desirable accuracy for the optimization of gas turbines blade-tip radial running clearance. Wong et al. [30] applied Fourier series for the uncertain reliability analysis of turbine blade disks, and proved that its accuracy and efficiency are acceptable. Bai et al. [31] developed an efficient multi-stage multi-disciplinary model based on a dynamic substructure method for turbine blisk, and indicated that the computational efficiency and accuracy of the proposed approach are better than support vector regression. Lin et al. [32] proposed a model for reliability analysis of aeroengine blade considering fatigue failure mode, and demonstrated that the proposed model was reasonable and matched with real-system conditions. An et al. [33] used the stress–strength interference (SSI) model for the reliability analysis of aeroengine decelerator regarding random variables. Fei et al. [24] applied extremum response surface method (ERSM) -based support vector machine (SVM) for optimum design of blade-tip radial running clearance in respect of nonlinear properties of materials and thermal loads. Lu et al. [34] developed a multi-extremum response surface method (MERSM) for the reliability analysis of aeroengine turbine blisk considering multiple failure modes, and illustrated the good performance of MERSM in accuracy and efficiency. Zhang et al. [35, 36] applied improved RSM considering the effect of strain and stress, gas temperature and gas velocity, to study on low cycle fatigue and high-temperature creep of turbine blisk. Fei et al. [15] proposed a surrogate model method for the reliability analysis and robust design of turbine blisk. Wang et al. [37] investigated the parameters of BTC for different rotating speed and active clearance control (ACC) of aeroengines. Zuo et al. [38] studied the reliability of aeroengine oil system using evidential network model based fault tree analysis considering epistemic uncertainty. To reduce the computational burden of complex problems, the modeling method basis multi-extremum surface of failure regions is significantly reduced computational times to evaluate failure domains. The main change in modeling methods is to provide the accurate prediction of multi-extremum performance functions under complex uncertainties. Although the RSM is one of simple and efficient regression tools, the abilities of the RSM for accurate estimation of multi-extremum basis functions have some limitations due to the usage of second-order polynomial function. The flexibility of RSM with respect to the nonlinear relationship for nonlinear dynamic responses potentially enhance to reach the efficient and accurate multi-extremum nonlinear relationships.

The objective of this paper is to develop an accurate surrogate model to determine the nonlinear responses of multi-failure modes of complex structures. In respect of this purpose, two novel modified multi-extremum response surface models (MRSM) are developed for the dynamic response of aeroengine turbine blisk. Moreover, a sensitivity analysis using MRSM is adopted to investigate the variation of input variables on the nonlinear responses. The remaining of this paper is structured as follows. In Sect. 2, the fundamentals of the two MRSMs are discussed. A general overview of turbine blisk specifications and dynamic analysis

are conducted in Sect. 3. Comparative modeling results are reported in Sect. 4. Section 5 summarizes some conclusions of this work.

2 Multi-extremum-modified response basis model

RSM is commonly applied to approximate to the failure modes of aeroengine structures under complex conditions in loads and manufacturing materials [15]. The ability of RSM to balance between accuracy and simplicity is one of the exciting characteristics in approximating complex engineering problems. The main effort in RSM is to provide a nonlinear relation as second-order basis polynomial functions between input variables (i.e., inlet temperature, material density, inlet velocity, and rotor speed) and outputs as multi-failure responses (i.e., blisk deformation, stress, and strain). The RSM cannot approximate highly nonlinear problems with high-correlation of input variables for complex problems due to approximating responses using polynomial function with quadratic form. Consequently, the accuracy of models, which is one of the major efforts in modeling process, is depended on the nonlinearity forms of approximated relation, input data points, training process, and parameters of models. In the current work, a multi-extremum-modified response model is proposed based on two calibrating processes. In the first modeling approach, each input variable is transferred based on a nonlinear mapping with power or exponential function, while the calibrating data points are provided by the first step, which is used for regressing the multi-extremum third-order polynomial functions. Figure 1 represents the modeling framework of two regressed RSM, denoted as MRSM. In this modeling approach, four layers of 1–4 are applied, including input layer (layer 1), normalized layer (layer 2), nonlinear mapping layer (layer 3) and calibrating layer (layer 4). The calibrating procedures using

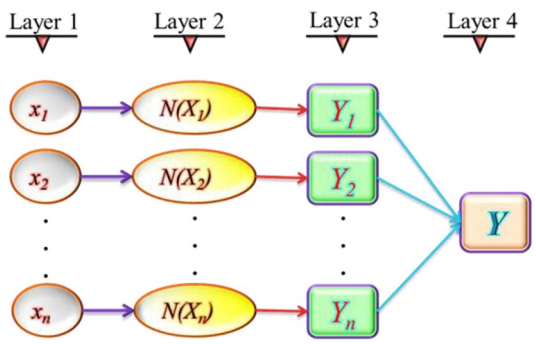

Fig. 1 The framework of multi-extremum-modified response basis model

the nonlinear response of turbine blisk under fluid-thermal uncertainties are given in layer 3 and layer 4.

As seen in Fig. 1, the results of MRSM are the approximated data (Y) of multi-failure modes of blisk deformation, stress, strain at layer 4 which are calibrated by input variables ($X=(x_1, x_2, \ldots, x_n)$), i.e., inlet temperature, inlet velocity, material density and rotor speed at layer 1. The details of layers 1–4 are expressed as follows:

Layer 1: Give input variable ($x_1, x_2, \ldots, x_n$) which are simulated using LHS with 150 sample in the train and 44 sample points in the test phases.

Layer 2: Normalize variables using the statistical properties of input variables [39], i.e.,

$$N(X) = \frac{X-\mu}{\sigma}, \tag{1}$$

where $N(X)$ presents the normal variable of X with mean of μ and standard diversion of σ, including temperature (T) ($\mu_T = 1164.94$ K, $\sigma_T = 26.01$ K), material density (ρ) ($\mu_\rho = 4450$ kg/m^3, $\sigma_\rho = 57.8$ kg/m^3), inlet velocity (v) ($\mu_v = 160$ m/s, $\sigma_v = 11.55$ m/s) and rotor speed (ω) ($\mu_\omega = 1150.1$ rad/s, $\sigma_\omega = 86.6$ rad/s), where μ and σ are computed based on simulated data points in training phase. In the normalized data, the standard deviation is a scale factor to control the range of the normalized input data. By normalizing input data, the free-dimensions of input data are used in the calibrating process. The large and small input bounds could be provided by the factor σ. The input data have a narrow bound when σ is minimal value, while a high-bound for input data is obtained as σ is large value.

The layers 1 and 2 are determined based on the input variables which are connected with the final layer. This connection is structured based on two significant calibrations, which are created in layers 3 and 4.

Layer 3: Mapping the normalized data based on the first regression procedure.

In the current work, two nonlinear mapping data points are presented to provide the nonlinear effects of input variables. In the first map, the linear function in the following equation is adopted to improve the RSM in MRSM-LN:

$$Y_i = a_{0i} + a_{1i} N(X_i). \tag{2}$$

In the second map, the exponential function, namely MRSM-EXP, is used as follows:

$$Y_i = a_{0i} + a_{1i} \exp\left[N(X_i)\right], \tag{3}$$

where a_{0i} and a_{1i} are the unknown coefficients.

The linear and exponential mapping data are used in the first calibrating process, which is provided by a connection between input data and output responses. Based on the calibrating, the input data are considered based on its influence that is determined by the coefficients a_{1i}. The unknown

coefficients are calculated using the dimensionless input variables, which are computed in layer 2. Therefore, a_1 and a_2 have the same dimensions for each input variable. Thus, the sensitivity of input variable is suggested by

$$\alpha_i = \frac{a_{1i}}{\sqrt{\sum_{i=1}^{n} \left(a_{1i}\right)^2}}, \tag{4}$$

where a_i ($i = 1, 2, \ldots, n$) denotes the sensitivity degree for variable x_i. In the proposed MRSM, the sensitivity analysis of input data is computed while the traditional RSM cannot handle input data as uncertainties. Moreover, the proposed model can be used as an acceptable guideline for robust design, controlling, and reliability analysis of complex structures. In this work, effective input variables are considered as the nonlinear response of dynamic turbine blisk failure modes.

The sensitivity degree of input variables is determined by the calibrating coefficients in the first stage. The flexibility of RSM is enhanced based on the transformation of input variables using linear and exponential maps.

Layer 4: Calibrate the nonlinear response of turbine blisk using the input mapping variables.

The approximated function of MRSMs using the linear and nonlinear maps are determined as [40]

$$f = a_0 + \sum_{i=1}^{n} a_i Y_i + \sum_{i=1}^{n} \sum_{j=i}^{n} a_{ij} Y_i Y_j, \tag{5}$$

where Y_i is the input data which are computed in the first calibrating process that is determined in layers 1–3. It is essential to compute the unknown coefficient $\boldsymbol{a} \in \{a_0, a_i, a_{ij}\ ,\ ij = 1, 2, ..., n\}$ that is commonly determined by least squared methodology via minimizing the error between computed nonlinear response ($\boldsymbol{O}$) and approximated function $(\boldsymbol{f})e = \left[\boldsymbol{O} - \boldsymbol{f}\right]^T \left[\boldsymbol{O} - \boldsymbol{f}\right]$ [15, 24], in which $\boldsymbol{f} = \boldsymbol{Pa}$ and $\boldsymbol{P}$ is the polynomial vector which is determined based on the mapping input data $Y \in \left\{Y_1, Y_2, ..., Y_n\right\}$ as below:

$$\boldsymbol{P} = \left[1,\ Y_1,\ Y_2, ...Y_n,\ Y_1^2,\ Y_1 Y_2, ..., Y_{n-1} Y_n, Y_n^2\right]. \tag{6}$$

The computed responses are determined based on the nonlinear dynamic finite-element model in respect of train dataset comprising 150 samples, denoted by $\boldsymbol{O} = \{o_1, o_2, ...o_{150}\}$. Thus, four input variables with 150 samples is used to train the models. The mapping input data points $\{Y_1, Y_2, ..., Y_n\}$ are computed by

$$\boldsymbol{Y} = \boldsymbol{P}_{xt}^T \left(\boldsymbol{P}_x^T \boldsymbol{P}_x\right)^{-1} \left(\boldsymbol{P}_x^T \boldsymbol{O}\right), \tag{7}$$

where $\boldsymbol{P}_x = [1, N(X)]$ for MRSM-LN and $\boldsymbol{P}_x = \left[1, \exp\left(N(X)\right)\right]$ for MRSM-EXP are train data, and $\boldsymbol{P}_{xt}$ is for test data points. The factors a_0, a_1 are computed using 150 train samples as $\left(\boldsymbol{P}_x^T \boldsymbol{P}_x\right)^{-1} \left(\boldsymbol{P}_x^T \boldsymbol{O}\right)$, by determining the first calibrating data in Eq. (7). The predicted value of a nonlinear response without the dynamic FE analysis is approximated by

$$\boldsymbol{f} = \boldsymbol{P}_t^T \left(\boldsymbol{P}^T \boldsymbol{P}\right)^{-1} \left(\boldsymbol{P}^T \boldsymbol{O}\right), \tag{8}$$

where $\boldsymbol{P}_t$ indicates the polynomial basis function for test data. Unlike the RSM, the proposed approach is established by the two main regressions procedures, while the MRSM is simply provided by sensitivity factors for each input variable. The accurate prediction of the nonlinear response for complex dynamic problems with nonlinear analysis is the main effort in modeling process.

Figure 2 illustrates the framework of the current work using MRSM. The computational effort in the structure to build a nonlinear model is provided by the simple framework without complicated relations. The high-flexibility as the nonlinearity of the input variables is enhanced based on the first calibrating process in layer 3. The nonlinear mapping data using the exponential function can be improved by the nonlinearity of relations between input data and computed dynamic responses.

3 Two-way fluid-thermal–structural analysis of turbine blisk

A high gas pressure turbine blisk of an aeroengine (in Fig. 3) under high temperature–speed is considered as the case study of this work. To completely simulate the performance

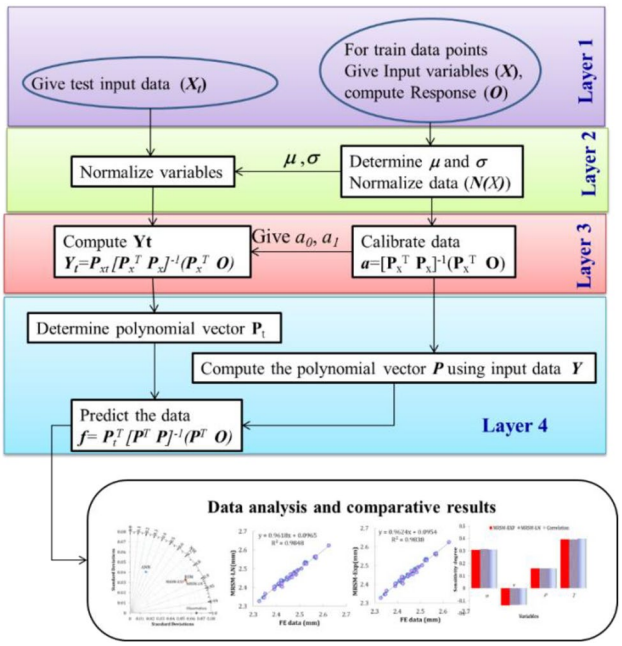

Fig. 2 The framework of MRSM basis nonlinear input map

Fig. 3 Aeroengine turbine blisk

Table 1 Temperature and speed value change with time

Time t, s	Temperature T, K	Rotate speed ω , rad/s	Time t, s	Temperature T, K	Rotate speed ω, rad/s
0	20	0	140	700	930
0.1	200	460	150	800	980
10	300	498	160	900	1168
95	400	627	165	1000	1168
100	500	725	200	1100	950
130	600	800	215	1150	950

of aeroengine, the flight profile and computing range are selected from start to cruise state [15, 41]. The Superalloy (Titanium alloy) is selected for the material of blisk. The analysis of blisk structure is performed by the fluid-thermal–structural coupling method considering nonlinear properties of materials and the dynamics of temperature and rotational speed. The time-dependent temperature load T and rotational speed ω are reported in Table 1.

3.1 Finite-element model

Turbine blisk is symmetrically typical. Thus, a single blisk could be considered as the object of simulation in Fig. 4. As shown in Figs. 4 and 5, the cooling hole of blade and convex platform of disk are selected to create a FE model of turbine blisk. The FE model of blisk consists of hexahedron and tetrahedron with 9 577 elements and 25 015 nodes, whiles the finite-volume (FV) model of flow field is built by hexahedron with 1 044 528 elements and 1 009 035 nodes.

Statistical properties of input variables for train and test data points, including rotating speed (ω), gas temperature (T), material density (ρ), and inlet velocity (v), are reported in Table 2, where $X_{\min}$, $X_{\max}$, X_{Mean}, and STD are, respectively, minimum, maximum, average, and standard deviation of input variables. The data in the train and test phases are

Fig. 4 FE model of the turbine blisk

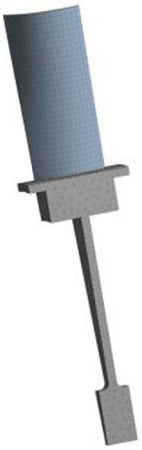

Fig. 5 FE model of the flow field

simulated by optimum Latin hypercube sampling with 150 points in train and 45 samples in test phases.

3.2 Nonlinear dynamic analysis of blisk

The deterministic analysis of blisk within the time domain [0, 215s] is summarized as follows:

(1) FV method is employed to investigate the fluid features of turbine blisk as the standard k-ε turbulence model.
(2) The law of energy conservation is used to resolve the thermodynamic property of flow flied in fluid-thermal analysis.
(3) FE method is employed to accomplish the structural analysis of turbine blisk and displacement function, geometric equation and constitutive equation are used to obtain analytical results based on shape equations of tetrahedron and hexahedron elements.
(4) The system coupling is used to actualize the solution of turbine blisk with fluid-thermal–solid interaction by multiple iterations and coupling information updating.

Table 2 Statistical characteristics of input variables for FE analysis

Variables	Train (150 data samples)				Test (44 data samples)			
	X_{min}	X_{max}	X_{Mean}	STD	X_{min}	X_{max}	X_{Mean}	STD
ω, rad·s^{-1}	1001	1299	1150.11	86.90	1125	1188	1156.66	14.49
V, m·s^{-1}	140.14	179.79	160.00	11.59	152.77	171.45	161.42	3.94
P, kg·m^{-3}	4351	4550.00	4449.98	58.00	4409	4495	4445.02	20.67
T, K	1120.20	1209.40	1164.94	26.10	1144.90	1186.50	1165.70	10.50

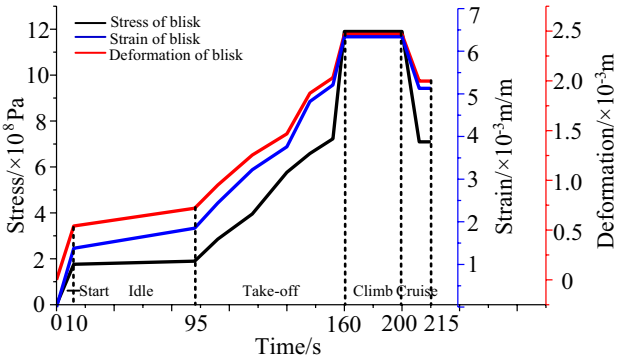

Fig. 6 Variation of deformation with time for turbine blisk

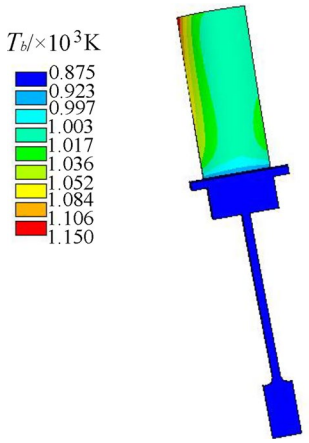

Fig. 8 Temperature distribution on turbine blisk

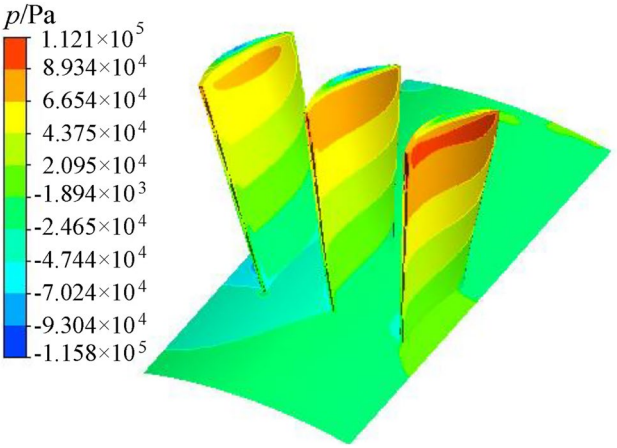

Fig. 7 Pressure distribution on the fluid-thermal–structure interface

From the two-way fluid-thermal–structural analysis of turbine blisk, the change curves of deformation, stress, and strain during the time domain are presented in Fig. 6.

As seen in Fig. 6, the maximum deformation, stress, and strain of turbine blisk are gained simultaneously at the time domain [160, 200 s]. The time point $t = 200$ s is considered as the critical point and computing point to estimate the safety of turbine blisk during the flight. Thus, the pressure distribution on the fluid-thermal–structural interface, the temperature distribution on turbine blisk, the nephograms of turbine blisk deformation, stress and strain, are shown in Figs. 7, 8, 9, respectively, in which p, T_b, u, σ, and ε indicate the pressure, temperature, deformation, stress, and strain values of turbine blisk, respectively.

As seen in Fig. 9, the maximum of blisk deformation emerges at the top of turbine blade, and the maximum values of blisk stress and strain are located at the bottom of the turbine blade.

To obtain modeling samples as train data and validated samples as test data generated by Latin hypercube sampling, three failure modes of turbine blisk, including maximum deformation, stress and strain are determined by nonlinear FE analysis regarding input variables. The data points of output responses of turbine blisk corresponding to the obtained input samples are acquired by two-way fluid-thermal–structural analyses. The statistical properties in training and test phases are listed in Table 3. The models are calibrated using training data, while the models performances are validated using the test dataset.

4 Comparative modeling results

The accuracy and agreement of the MRSM (i.e., MRSM-EXP and MRSM-LN) are compared with RSM, ANN models using four comparative statistics such as mean absolute error (*MAE*), root mean square error (*RMSE*), modified agreement index (d), and modified Nash and Sutcliffe efficiency (*NSE*) [42, 43], i.e.,

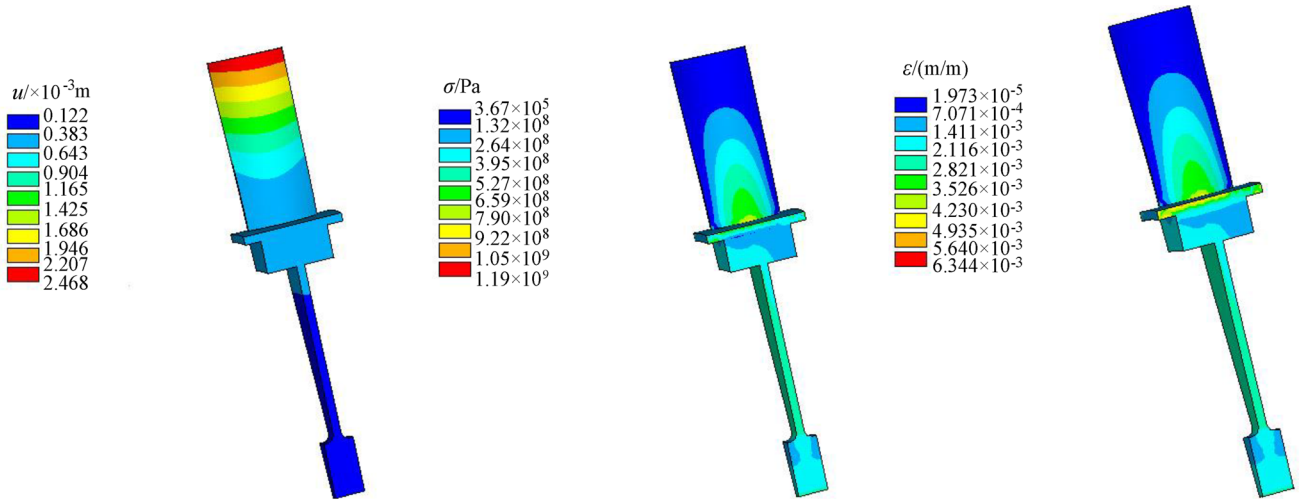

(a) Deformation of turbine blisk **(b)** Stress of turbine blisk **(c)** The strain of turbine blisk

Fig. 9 The nephograms of turbine blisk deformation

Table 3 Statistical characteristics of train and test data points for nonlinear responses of turbine blisk

Response	Train phase				Test phase			
	$X_{\min}$	$X_{\max}$	X_{Mean}	*STD*	$X_{\min}$	$X_{\max}$	X_{Mean}	*STD*
Deformation, mm	1.917	2.831	2.406	0.198	2.326	2.625	2.459	0.066
Stress, GPa	1.01	1.33	1.177	0.076	1.13	1.24	1.182	0.027
Strain, mm/mm	4.592	6.989	6.068	0.507	6.020	6.658	6.340	0.138

$$\text{RMSE} = \frac{1}{N}\sqrt{\sum_{i=1}^{N}[O_i - f_i]^2}, \tag{9}$$

$$\text{MAE} = \frac{1}{N}\sum_{i=1}^{N}|O_i - f_i|, \tag{10}$$

$$d = 1 - \frac{\sum_{i=1}^{N}|O_i - f_i|}{\sum_{i=1}^{N}|O_i - \overline{O}| + |f_i - \overline{O}|}\ ,\quad 0 < d \le 1, \tag{11}$$

$$\text{NSE} = 1 - \frac{\sum_{i=1}^{N}|O_i - f_i|}{\sum_{i=1}^{N}|O_i - \overline{O}|}\ ,\quad -\infty < \text{NSE} \le 1, \tag{12}$$

where N denotes the number of data; O_i and P_i are, respectively, i-th data point for computed FE responses and predicted models; $\overline{O}$ is the average of computed data using nonlinear dynamic FE. The RMSE and MAE values for each model are tended to zero. Thus, it can be induced that the predicted model relates to accurate predictions with minimum errors. d varies from 0 to 1 with no-correlation by the perfect fitness. The NSE presents the goodness-of-fitness of the model where NSE = 1 indicates perfect agreement predictions. These different statistics are determined for the train and test data points for blisk deformation, stress, and strain which are presented in Table 4. The ANN models is structured with 4 nodes in input layers, 4–10 nodes in the hidden layer which is obtained by trial and errors as 5, 7 and 8 nodes for blisk deformation, stress and strain, respectively. The bold numbers in the table are the best model. The results presented in Table 4 indicated that two modified models using linear and exponential maps are enhanced the performances of RSM for both accuracy (lowest RMSE, MAE) and agreement (highest d and NSE) for train and test phases. It can be conducted that ANN model is performed with worst abilities for all failure modes. Using MRSM-EXP, *MAE* (*RMES*) is enhanced about 82% (85%) and 77% (78%) for blisk deformation and about 24% (29%) and 10% (9%) for stress by comparing RSM and MRSM-LN models, respectively. The two regression processes in proposed MRSM models are improves the abilities of RSM for approximating the failure modes of this complex problem. It is suggested that the MRSM-LR and MRSM-EXP models are applied to simulate the performances of structure reliability design analyses in the future. Commonly, three failure modes of turbine blisk are predicted with the accurate results and acceptable agreement using MRSM-EXP compared to other models.

Table 4 Comparative statistics for different models of multi-nonlinear response in test and train datasets

Failure modes	Models	Train (150 points)				Test (44 points)			
		MAE	RMSE	*d*	NSE	MAE	RMSE	*d*	NSE
Blisk deformation, mm	RSM	0.520	0.644	0.998	0.997	7.394	10.863	0.972	0.928
	MRSM-LN	0.504	0.621	0.998	0.997	**6.546**	**8.596**	**0.983**	**0.936**
	MRSM-EXP	**0.285**	**0.348**	**0.999**	**0.998**	6.820	8.952	0.981	0.933
	ANN	68.919	84.740	0.744	0.583	33.458	39.597	0.633	0.658
Stress (MPa)	RSM	2.931	3.566	0.977	0.954	3.282	4.570	0.923	0.848
	MRSM-LN	2.610	3.026	0.980	0.959	2.947	3.926	0.931	0.863
	MRSM-EXP	**2.369**	**2.772**	**0.981**	**0.963**	**2.913**	**3.987**	**0.931**	**0.865**
	ANN	24.655	30.111	0.764	0.613	8.020	9.832	0.780	0.627
Strain (mm/m)	RSM	0.024	0.031	0.971	0.941	0.016	0.023	0.923	0.842
	MRSM-LN	0.017	0.017	0.980	0.959	**0.012**	0.016	0.942	0.885
	MRSM-EXP	**0.000**	**0.000**	**1.000**	**0.999**	**0.012**	**0.015**	**0.943**	**0.887**
	ANN	0.123	0.163	0.830	0.702	0.099	0.104	0.564	0.049

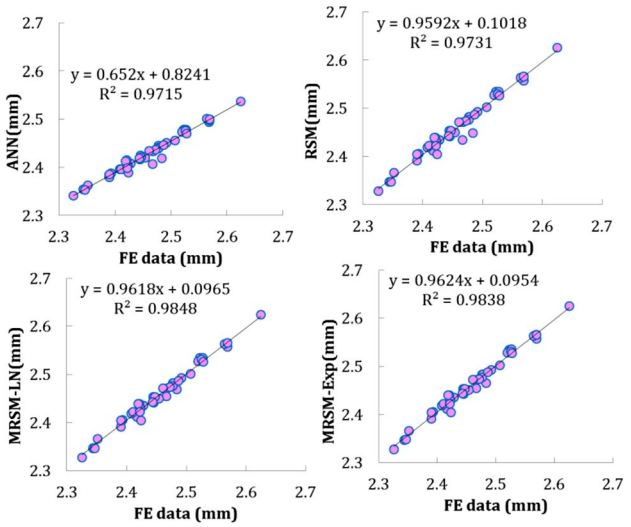

Fig. 10 Scatterplot for blisk deformation in test data

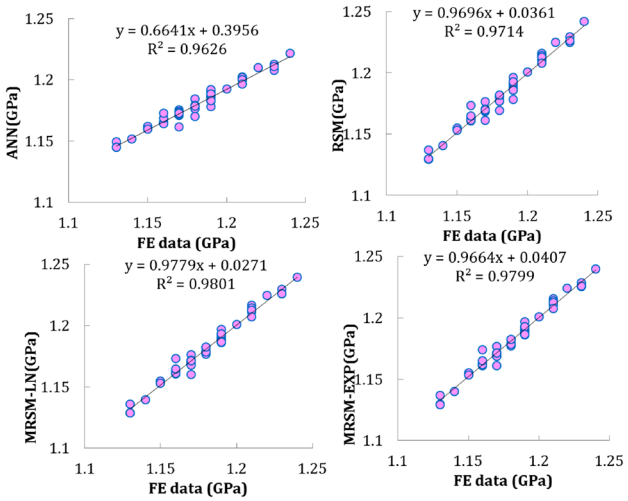

Fig. 11 Scatterplot for stress in test data

The scatterplot of test data between FE response and predicted models for blisk deformation are presented in Fig. 10. In this figure, R^2 is the correlations between the computed and predicted data points for different models. The larger value for R^2 denotes to higher tendency between predicted data and computed points. The scatterplot diagram for different models in the approximation of the test data for stress and strain are presented in Figs. 11 and 12, respectively. From the results of Fig. 10, the best and worst models are the MRSM-LN and ANN, respectively, against the other models. Moreover, the ability of MRSM-EXM is similar to the MRSM-LR and it is more robust and accurate than the RSM.

The scatterplot of test data for stress and strain in Figs. 11 and 12 demonstrated that the MRSM models with nonlinear exponential map enhances the abilities of MRSM to provide a nonlinear relation, compared to the RMS and ANN. The linear

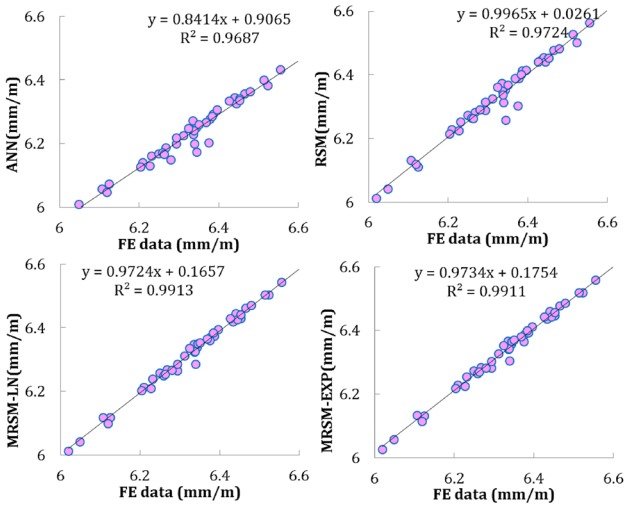

Fig. 12 Scatterplot for strain in test data

cross-correlations using second-order terms in RSM, i.e., Y_iY_j can improve the accuracy of the models while it is not applied in ANN. It can be conducted that artificial intelligent models basis ANN relations are required to improve their structures in training phase such as nonlinear active functions or input data as cross-terms, in the future.

The Taylor diagram basis standard deviations and *NSE* is illustrated in Fig. 13 for the test database of three failure modes of (a) blisk deformation, (b) stress, and (c) strain. As seen in Fig. 13, the computed data point using nonlinear dynamic FE is shown with the gray point on the horizontal line. The Taylor diagram in Fig. 13 indicates that the ANN models generally provide less performances than RSM and MRSM. However, the MRSM showed close predictions for blisk deformation and stress with the highest agreement index. The MRSM-EXP provided most accurate and robust predictions for strain data compared to RSM and MRSM-LN. Form the results of the Taylor diagram, it can be conducted that the models from best to worst predictions could be listed by following models of MRSM-EXP, MRSM-LN, RSM and ANN.

The effects of input variables can be evaluated based on the correlation coefficient with responses of failure modes in turbine blisk. Thus, it is defined as the sensitivity factor for each input data [44]:

$$\begin{cases} \alpha_i = \dfrac{r_i}{\sum_{i=1}^{n} |r_i|} \\ r = \dfrac{N\sum_{i=1}^{N} O_i x_i - \left[\sum_{i=1}^{N} O_i\right]\left[\sum_{i=1}^{N} x_i\right]}{\sqrt{N\sum_{i=1}^{N} O_i^2 - \left[\sum_{i=1}^{N} O_i\right]^2}\sqrt{N\sum_{i=1}^{N} x_i^2 - \left[\sum_{i=1}^{N} x_i\right]^2}} \end{cases}, \quad i = 1, 2, ..., n$$

where α is sensitivity degree; N and n indicate the numbers of data points and input variables, respectively; O is the response of turbine blisk; x is the input variable. The sensitivity degree based on correlation and the proposed MRSM is compared with respect of the same input variables (ω, v, ρ, and T). The results for sensitivity degree of input variables are presented in Fig. 14 for relative failure modes. It can be seen that the strong agreements are provided by the exponential and linear relations with the correlation sensitivity degree. The sensitivity frameworks in the proposed modeling approach can accurately evaluate the importance of input variables. By comparing the sensitivity of blisk deformation, stress, and strain performance functions, the temperature provides highest effects on the nonlinear responses of the failure modes, while rotor speed as the load of the problem is positively affected in Layer 2 for deformation and strain failure modes. Inlet velocity adversely effects on the performances of studied failure modes, while other input variables of ω, ρ and T hold positive effects. The different sensitivity values of inlet velocity are computed for each model. It is obtained that inlet velocity significantly influences the performances of blisk deformation and stress, while it is insensitive on the strain and blisk deformation is more sensitive than v.

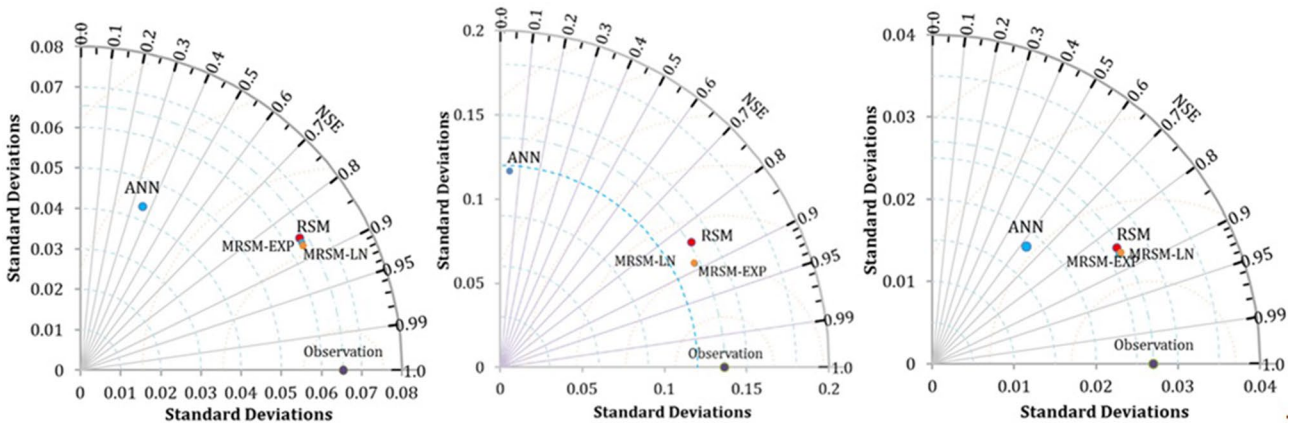

Fig. 13 Taylor diagram for test data (**a**) blisk deformation, (**b**) stress and (**c**) strain

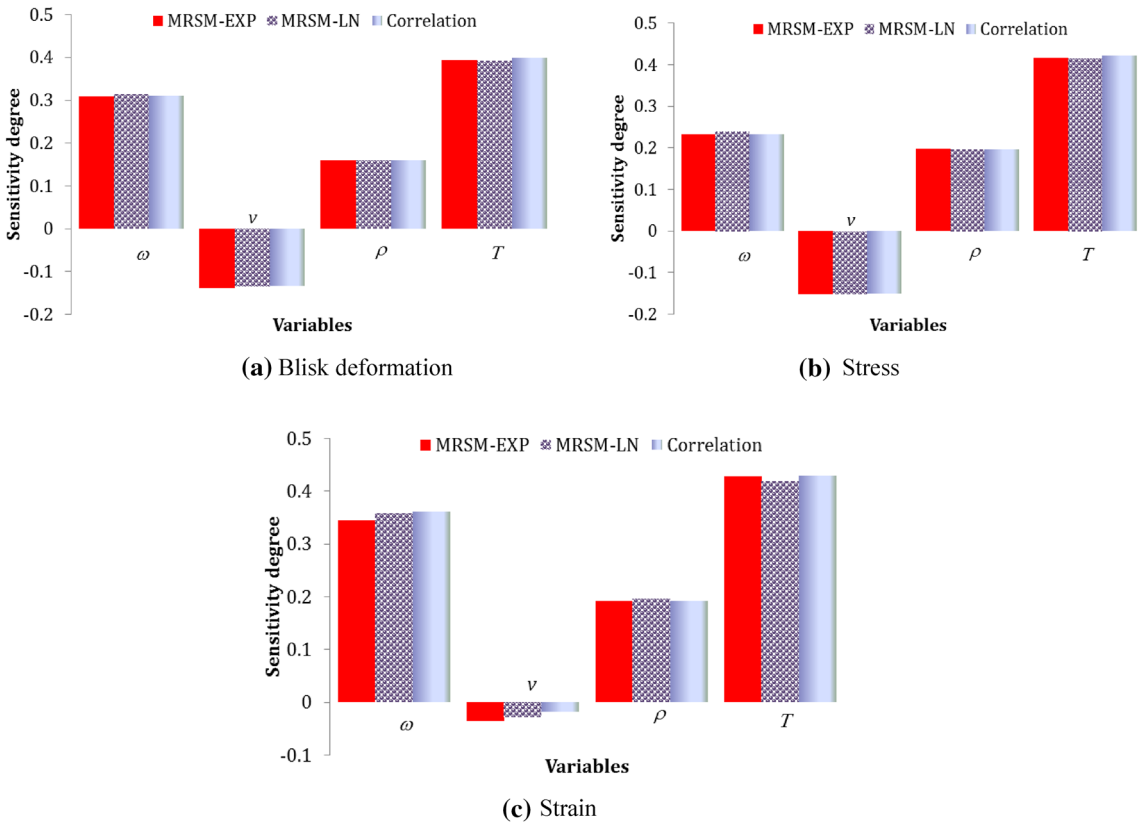

Fig. 14 Sensitivity degree of input variables using correlation and MRSM. **a** Blisk deformation, **b** stress and **c** strain

5 Conclusions

The main effort in this work was to develop a modified multi-extremum response (MRSM) to approximate the multi-failure nonlinear dynamic responses of aeroengine components under high-temperature and rotating speed loads, with regard to fluid-thermal–structure interaction. Two multi-extremum-modified response basis models are established based on two regressing processes. In the first regression phase, the exponential and linear functions are used to calibrate the input variable. In respect of the acquired calibrating results, it is a fast and straightforward sensitivity analysis during the modeling process. The influences of input variables on multi-failure modes are investigated using the proposed sensitivity factors. The abilities of the proposed MRSM models coupled with linear (MRSM-LN) and exponential (MRSM-EXP) mappings are compared with RSM and ANN. Compared results indicated that the proposed sensitivity vector for linear and exponential functions reveals the largest influence of gas temperature, following by angular speed and material density. At the same time, inlet velocity is an insensitive parameter for maximum strain. Two models of MRSM-LN and MRSM-EXP have superior performances compared to RSM and ANN. The proposed MRSM is a promising approach in approximating and simulating in optimization, reliability analysis and reliability-based design optimization of the complex structures under multi-failure response in future.

Acknowledgements This paper is co-supported by the National Natural Science Foundation of China (Grant nos. 51975124), Shanghai Belt and Road International Cooperation Project of China (Grant No. 20110741700) and University of Zabol (Grant no. UOZ-GR-9618-1). The authors would like to thank them. The Deanship of Scientific Research (DSR) at King Abdulaziz University, Jeddah, Saudi Arabia has funded this project under grant no. (FP-214-42).

Compliance with ethical standards

Conflict of interests The authors declare that there is no conflict of interest regarding the publication of this article.

References

1. Meguid S, Mao R, Ng T (2008) FE analysis of geometry effects of an artificial bird striking an aeroengine fan blade. Int J Impact Eng 35(6):487–498

2. Qi XM, Piao Y, Zhu JH, Zhou JX (2008) 3-D numerical analysis of the tip clearance of an aero-engine high pressure turbine. J Aerospace Power 5:904–908
3. Dong W, Zhu J, Zhou Z, Chi X (2015) Heat transfer and temperature analysis of an aeroengine strut under icing conditions. J Aircraft 52(1):216–225
4. Szwaba R, Kaczynski P, Doerffer P, Telega J (2016) Flow structure and heat exchange analysis in internal cooling channel of gas turbine blade. J Therm Sci 25(4):336–341
5. Peschiulli A, Coutandin D, Del Cioppo M, Damasio M Development of a numerical procedure for integrated multidisciplinary thermal-fluid-structural analysis of an aeroengine turbine. In: ASME Turbo Expo 2009: Power for Land, Sea, and Air, 2009. American Society of Mechanical Engineers Digital Collection, pp 1253–1262.
6. Satish T, Murthy R, Singh A (2014) Analysis of uncertainties in measurement of rotor blade tip clearance in gas turbine engine under dynamic condition. Proc Inst Mech Eng Part G 228(5):652–670
7. Zhai X, Fei CW, Choy YS, Wang JJ (2017) A stochastic model updating strategy-based improved response surface model and advanced Monte Carlo simulation. Mech Syst Signal Process 82:323–338
8. Lu C, Feng YW, Fei CW, Bu SQ (2020) Improved decomposed-coordinated Kriging modeling strategy for dynamic probabilistic analysis of multi-component structures. IEEE Trans Reliab 69(2):440–457
9. Keshtegar B, Hao P, Wang Y, Li Y (2017) Optimum design of aircraft panels based on adaptive dynamic harmony search. Thin-Walled Struct 118:37–45
10. Fei CW, Liu HT, Zhu ZZ, An LQ, Li SL, Lu C (2021) Whole-process design and experimental validation of landing gear lower drag stay with global/local linked driven optimization strategy. Chin J Aeronaut Online,. https://doi.org/10.1016/j.cja.2020.07.035
11. Fei CW, Liu HT, Li SL, Li H, An LQ, Lu C(2020). Dynamic parametric modeling-based model updating strategy of aeroengine casings. Chin J Aeronaut, accepted.
12. Gaspar B, Teixeira A, Soares CG (2017) Adaptive surrogate model with active refinement combining Kriging and a trust region method. Reliability Eng Syst Saf 165:277–291
13. Xiao M, Zhang J, Gao L (2020) A system active learning Kriging method for system reliability-based design optimization with a multiple response model. Reliability Eng Syst Saf 199:106935. https://doi.org/10.1016/j.ress.2020.106935
14. Xiao NC, Yuan K, Zhou C (2020) Adaptive kriging-based efficient reliability method for structural systems with multiple failure modes and mixed variables. Comput Methods Appl Mech Eng 359:112649
15. Fei CW, Lu C, Liem RP (2019) Decomposed-coordinated surrogate modeling strategy for compound function approximation in a turbine-blisk reliability evaluation. Aerosp Sci Technol 95:105466
16. Lu C, Fei CW, Li H, Liu HT, An LQ (2020) Moving extremum surrogate modeling strategy for dynamic reliability estimation of turbine blisk with multi-physics fields. Aerosp Sci Technol 106:106112
17. Zhang J, Xiao M, Gao L, Fu J (2018) A novel projection outline based active learning method and its combination with Kriging metamodel for hybrid reliability analysis with random and interval variables. Comput Methods Appl Mech Eng 341:32–52
18. Zhang J, Xiao M, Gao L, Qiu H, Yang Z (2018) An improved two-stage framework of evidence-based design optimization. Struct Multidisciplinary Opt 58(4):1673–1693
19. Goswami S, Ghosh S, Chakraborty S (2016) Reliability analysis of structures by iterative improved response surface method. Struct Saf 60:56–66
20. Dai H, Zhang H, Wang W (2012) A support vector density-based importance sampling for reliability assessment. Reliability Eng Syst Saf 106:86–93
21. Fei CW, Li H, Liu HT, Lu C, An LQ, Han L, Zhao YJ (2020) Enhanced network learning model with intelligent operator for the motion reliability evaluation of flexible mechanism. Aerosp Sci Technol 107:106342
22. Xiao M, Gao L, Xiong H, Luo Z (2015) An efficient method for reliability analysis under epistemic uncertainty based on evidence theory and support vector regression. J Eng Des 26(10–12):340–364
23. Zhang J, Xiao M, Gao L, Chu S (2019) Probability and interval hybrid reliability analysis based on adaptive local approximation of projection outlines using support vector machine. Comput-Aided Civ Infrastruct Eng 34(11):991–1009
24. Fei CW, Li H, Liu HT, Lu C, Keshtegar B (2020) Multilevel nested reliability-based design optimization with hybrid intelligent regression for operating assembly relationship. Aerospace Sci Technol:105906.
25. Keshtegar B, Kisi O (2017) M5 model tree and Monte Carlo simulation for efficient structural reliability analysis. Appl Math Modelling 48:S0307904X17301439.
26. Seghier MEAB, Keshtegar B, Correia JA, Lesiuk G, De Jesus AM (2019) Reliability analysis based on hybrid algorithm of M5 model tree and Monte Carlo simulation for corroded pipelines: case of study X60 Steel grade pipes. Eng Fail Anal 97:793–803
27. Chojaczyk A, Teixeira A, Neves LC, Cardoso J, Soares CG (2015) Review and application of artificial neural networks models in reliability analysis of steel structures. Struct Saf 52:78–89
28. Hu DY, Yang JJ, Fei CW, Wang RQ, Choy YS (2017) Reliability-based design optimization method of turbine disk with transformed deterministic constraints. J Aerospace Eng 30(1):04016070
29. Fei CW, Bai GC (2014) Distributed collaborative probabilistic design for turbine blade-tip radial running clearance using support vector machine of regression. Mech Syst Signal Process 49(1–2):196–208
30. Wong CN, Huang HZ, Li N (2013) Fourier series based reliability analysis of aeroengine turbine blade under linear fuzzy safety state. Eng Fail Anal 31:268–280
31. Bai B, Bai GC, Li C (2015) Application of multi-stage multi-objective multi-disciplinary agent model based on dynamic substructural method in Mistuned Blisk. Aerosp Sci Technol 46:104–115
32. Lin J, Zhang J, Yang S, Bi F (2013) Reliability analysis of aeroengine blades considering nonlinear strength degeneration. Chin J Aeronaut 26(3):631–637
33. An Z, Huang H, Wang Z, Zhang X, Wang G (2010) Discrete stress-strength interference model of reliability analysis under multi-operating conditions. Chin J Mech Eng 23(3):398–402
34. Lu C, Feng YW, Fei CW, Xue XF (2018) Probabilistic analysis method of turbine blisk with multi-failure modes by two-way fluid-thermal-solid coupling. Proc Inst Mech Eng Part C 232(16):2873–2886
35. Zhang CY, Lu C, Fei CW, Liu LJ, Choy YS, Su XG (2015) Multiobject reliability analysis of turbine blisk with multidiscipline under multiphysical field interaction. Advances in Materials Science and Engineering 2015.
36. Zhang CY, Wei JS, Wang Z, Yuan ZS, Fei CW, Lu C (2019) Creep-based reliability evaluation of turbine blade-tip clearance with novel neural network regression. Materials 12(21):3552
37. Wang W, Shao H, Shao X, Song K Investigation on the turbine blade tip clearance measurement and active clearance control based on eddy current pulse-trigger method. In: ASME Turbo Expo 2017: Turbomachinery Technical Conference and

Exposition. American Society of Mechanical Engineers Digital Collection.
38. Zuo L, Xiahou T, Liu Y (2019) Evidential network-based failure analysis for systems suffering common cause failure and model parameter uncertainty. Proc Inst Mech Eng Part C 233(6):2225–2235
39. Keshtegar B, Meng D, Ben Seghier MEA, Xiao M, Trung NT, Bui DT (2020) A hybrid sufficient performance measure approach to improve robustness and efficiency of reliability-based design optimization. Eng Comput. https://doi.org/10.1007/s00366-019-00907-w
40. Zhu S-P, Keshtegar B, Tian K, Trung N-T (2021) Optimization of load-carrying hierarchical stiffened shells: comparative survey and applications of six hybrid heuristic models. Arch Comput Methods Eng. https://doi.org/10.1007/s11831-021-09528-3
41. Fei CW, Choy YS, Hu DY, Bai GC, Tang WZ (2016) Transient probabilistic analysis for turbine blade-tip radial clearance with multi-component and multi-physics fields based on DCERSM. Aerosp Sci Technol 50:62–70
42. Bai B, Li H, Zhang W, Cui YC (2020) Application of extremum response surface method-based improved substructure component modal synthesis in mistuned turbine bladed disk. J Sound Vib 472:115210. https://doi.org/10.1016/j.jsv.2020.115210
43. Nehdi ML, Keshtegar B, Zhu SP (2019) Nonlinear modeling for bar bond stress using dynamical self-adjusted harmony search optimization. Eng Comput. https://doi.org/10.1007/s00366-019-00831-z
44. Kowsar R, Keshtegar B, Miyamoto A (2019) Understanding the hidden relations between pro-and anti-inflammatory cytokine genes in bovine oviduct epithelium using a multilayer response surface method. Sci Rep 9(1):1–17